Analyzing and Improving Cartesian Stiffness Control Stability of Series Elastic Tendon-driven Robotic Hands

Prashant Rao and Ashish D. Deshpande

***Abstract*— Robust and dexterous manipulation is identified as one of the critical challenges in the field of robotic hand design and control. A key requirement of dexterous manipulation is the ability to modulate fingertip force directions and magnitudes. Cartesian stiffness control is a strategy to generate position dependent fingertip forces. However the stability conditions for the Cartesian stiffness controllers vary nonlinearly because of dependency on the manipulator's configuration and loading forces. The challenge is enhanced in case of tendon-driven robotic hands due to passive joint coupling. In this work, we derive a generalized passivity based stability boundary for Cartesian stiffness. We then present a methodology to analyze the stability boundaries of Cartesian stiffness controlled series elastic tendon-driven robotic fingers. We also present a solution to improve stability by optimizing the arrangement of optimized passive compliance in parallel to the actuators based on the stability criteria. Our analysis not only allows for informed design of new robotic hands but also applies to improving performance of existing robotic hands.**

I. Introduction

Dexterous in-hand manipulation is one of the biggest challenges in the field of robotics. Over the past two decades, many strategies have been implemented towards improving object manipulation capabilities of robotic hands [1], [2]. Dexterous manipulation requires accurate control of fingertip force magnitudes and directions. Cartesian stiffness control is a control strategy to accurately and robustly control forces/torques and positions of fingertips.

Cartesian stiffness control allows the generation of position dependent fingertip forces which are considered beneficial for manipulation. Stability of such controllers have been analyzed for systems with decoupled passive joint stiffnesses such as robotic arms [3], [4], [5]. However, compliant tendon-driven robots have passively coupled joints due to tendon routing constraints. As tendons route through many joints, such robots have fully populated stiffness matrices. Cartesian stiffness stability for such robots has not been analyzed. Specifically, there are two factors that could make such systems unstable: configuration dependency and loading forces, both of which are encountered during manipulation. Thus, it becomes important to analyze stability for such systems to understand and improve robotic manipulation.

In our previous work [6], we presented a generalized proof of a passivity based stability criteria for compliant tendon-driven multi-degree of freedom (DOF) robotic fingers implementing joint stiffness controllers. In this work, we extend our stability criteria to Cartesian stiffness controllers. Through analysis and simulations, we show that due to the configuration dependency of such controllers, a controller stiffness that might be stable in one area of the workspace might be unstable in another. We further show that addition of external forces adds another facet to Cartesian stability, due to a configuration dependent force based joint stiffness known as conservative congruency transformation (CCT)[7].

We present a solution to improve manipulation performance and stability by utilizing the mechanical arrangements of passive compliance. While researchers have worked on improving manipulation capabilities of robotic hands by different means such as sensors, kinematics and controllers [1], [2], we are more interested in exploiting the arrangements of passive compliance in tendon-driven hands to provide intrinsic stability to augment controllers. Towards that goal, we identified compliance arranged in parallel to actuators (parallel compliance) as a useful design parameter in our previous work [8], [9] which can be optimized to improve stability. We present a method to choose an optimal set of constant stiffness springs in parallel to the actuators at the joints that mitigate the instability due to configuration and external forces. Addition of the springs also improves the overall workspace utilization and stability of robotic fingers intrinsically by virtue of mechanical design.

II. Stability Bounds of Cartesian Stiffness Control

In our previous work [6] we analyzed the stability boundaries of joint stiffness control for series-elastic tendon-driven robotic hands with coupled (fully populated) passive joint stiffness which can mathematically be represented as,

$$\mathbf{K_{j,passive}} = \mathbf{R^T K_{sc} R} + \mathbf{K_{pc}} \tag{1}$$

where $\mathbf{R}$ is the transformation matrix from joint space to tendon space also known as the moment arm matrix defining the tendon routing strategy. $\mathbf{K_{sc}}$ is the diagonal matrix of tendon stiffness and $\mathbf{K_{pc}}$ is the parallel compliance at the joints.

We showed that for a generalized multi-DOF series elastic tendon driven system with fixed passive joint stiffness and a constant joint stiffness controller gain ($\mathbf{K_{j,d}}$), the passivity boundaries can be expressed as,

$$\mathbf{K_{j,passive}} - \mathbf{K_{j,d}} \geq \mathbf{0} \tag{2}$$

$$\mathbf{K_{j,d}} > \mathbf{K_{pc}} \tag{3}$$

In other words, to maintain passivity, the maximum allowable joint controller gain (controller joint stiffness) has to be

This work was supported by NSF Grant 1157954. All authors are with the Department of Mechanical Engineering, University of Texas at Austin, Austin, TX, USA. Send correspondence to prashant.rao@utexas.edu

bounded by the net passive stiffness of the system. If the series elastic springs have constant stiffness and the routing pulleys are circular, the joint stiffness stability bounds are invariant of robot configuration or constant over the entire workspace.

Cartesian stiffness controllers are fundamentally different from joint space controllers primarily because of the configuration dependency of controller torques. To have a better understanding of stability bounds of Cartesian stiffness control, we revisit the principle of virtual work relating Cartesian forces to joint torques.

$$\boldsymbol{\tau} = \mathbf{J^T(q)f_x} \tag{4}$$

where $\boldsymbol{\tau}$ is the vector of joint torques, $\mathbf{q}$ is the vector of joint angles, $\mathbf{J}$ is the Jacobian transformation matrix from Cartesian space to joint space and $\mathbf{f_x}$ is the vector of Cartesian end-tip forces.

Stiffness is defined as the rate of change of torque with respect to joint angle. Differentiating the above equation with respect to joint angle yields,

$$\mathbf{K_j} = \mathbf{J^T(q)K_xJ(q)} + \frac{\delta \mathbf{J^T(q)}}{\delta \mathbf{q}}\mathbf{f_x} \tag{5}$$

where the first term is the transformation of Cartesian end-tip stiffness ($\mathbf{K_x}$) to joint space stiffness ($\mathbf{K_j}$) invariant of external forces. The second term is a configuration dependent external force based stiffness term (CCT). We will address this stiffness term as $\mathbf{K_{j,CCT}}$ for simplicity.

When no external forces are acting on the system, the transformation can be rewritten as,

$$\mathbf{K_j} = \mathbf{J^T(q)K_xJ(q)} \tag{6}$$

Thus, the joint stiffness of a system can be expressed in Cartesian space as

$$\mathbf{K_x} = \mathbf{J^{-T}(q)K_jJ^{-1}(q)} \tag{7}$$

Multiplying both equations of the joint stiffness stability criteria (Eq.(2) and (3)) by $\mathbf{J^{-T}(q)}(...)\mathbf{J^{-1}(q)}$ on both sides,

$$\mathbf{J^{-T}(q)K_{j,passive}J^{-1}(q) - J^{-T}(q)K_{j,d}J^{-1}(q) \geq 0} \tag{8}$$

$$\mathbf{J^{-T}(q)K_{j,d}J^{-1}(q) > J^{-T}(q)K_{pc}J^{-1}(q)} \tag{9}$$

Using Eq. (7), the joint stiffness criteria can be transformed to Cartesian stiffness control stability bounds,

$$\mathbf{K_{x,passive}(q) - K_{x,d} > 0} \tag{10}$$

$$\mathbf{K_{x,d} \geq J^{-T}(q)K_{pc}J^{-1}(q)} \tag{11}$$

where $\mathbf{K_{x,passive}}$ is the net passive Cartesian stiffness of the system. As the joint stiffness stability criteria accounts for fully populated passive stiffness matrices, it can thus be reliably used to derive the Cartesian stiffness stability criteria,

For systems with external forces acting on the finger-tip, the passive stiffness can be rewritten as,

$$\mathbf{K_{x,passive}(q) = J^{-T}(q)(K_{j,passive} - K_{j,CCT})J^{-1}(q)} \tag{12}$$

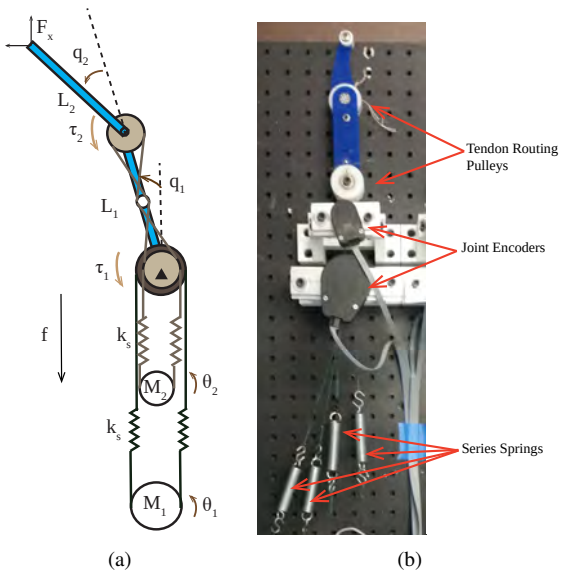

(a) (b)

Fig. 1. (a) A 2-DOF tendon-driven planar robotic finger with tendon stiffness of k_{sc} on all tendons [6]. Two motors (M_1 and M_2) actuate the two DOFs using a belt-drive (2N) strategy. The tendons for the second joint route through an idler pulley on the first joint, resulting in compliant coupling between both joints. (b) Experimental equivalent 2-DOF testbed for validating the system analysis. The experimental system follows the same routing strategy as the simulation system

The criteria dictates that the maximum achievable controller stiffness is always bounded by the passive stiffness of the system to maintain actuator passivity. As the passive stiffness matrix is fully populated, the inequality is treated as a test of positive definiteness rather than an element-wise subtraction. We see that when constant passive joint stiffness is transformed to Cartesian space, it is a nonlinear function of both configuration and external forces thus making the stability bounds to vary at different points in the workspace.

III. Analyzing Stable Cartesian Workspace

We are interested in understanding the effects of configuration and force dependency on stability boundaries. Thus, we performed an analysis on stability over the Cartesian workspace for fixed controller stiffness values. The analysis was performed for both unloaded and loaded systems.

A. Cartesian Stiffness Control

The stability bounds presented are generalized and hence can be applied to any series elastic tendon-driven robot. However for this study, we model a planar 2-DOF robotic finger with a modified 2N (N is the DOFs) tendon routing in the form of a belt drive and series springs of equal stiffness on the joints (Fig. 1).

To generate Cartesian end-tip stiffness ($\mathbf{K_{x,d}}$) with its resting position at ($\boldsymbol{x_d}$), the controller can be designed as,

$$\boldsymbol{\tau_d} = \mathbf{J^T(\theta)(K_{x,d}(x_d - x))} \tag{13}$$

Now that a desired joint torque ($\boldsymbol{\tau_d}$) has been estimated, the tendon level controller has to calculate the actuator displacement ($\boldsymbol{\theta_d}$) required to generate the desired torque.

The tendon forces can be estimated by

$$\mathbf{f_t} = \mathbf{K_{sc}}(\mathbf{R_m}\boldsymbol{\theta} - \mathbf{Rq}) \tag{14}$$

where $\mathbf{R_m}$ is the diagonal matrix of motor pulley radii and $(\boldsymbol{\theta})$ is the vector of motor angles.

Forces can be generated using series compliance by creating appropriate displacements by the actuator. Without loss of generality, we can assume that the motor has a closed-loop, tuned position controller implemented which makes its response equal to a first order system which can be modeled as,

$$\dot{\boldsymbol{\theta}} = \frac{\mathbf{1}}{\boldsymbol{t_r}}(\boldsymbol{\theta_d} - \boldsymbol{\theta}) \tag{15}$$

where, $\theta_\mathbf{d}$ is the desired motor position and $\mathbf{t_r}$ is the rise time of the first order response.

Thus using, Eq. (13), (14) and (15), the required motor displacement for generating controller torques can be calculated.

B. Stable Workspace of Unloaded Fingers

We begin by assuming no external forces acting on the finger. We chose a feasible rectangular area of the overall finger workspace (dashed-line region) and then picked nine points within that workspace to denote an example manipulation task workspace (Fig. 2). Three decoupled (diagonal) controller stiffnesses were picked to emulate various manipulation task scenarios. The first case is high stiffness in x-direction and low in y-direction. The second is high stiffness in y-direction and low in x-direction. Finally we chose equal controller stiffness in both directions. The first two controller stiffnesses are for tasks where accuracy (high stiffness) is required in one direction while robustness against external impacts (low stiffness) is required in the other. Isotropic stiffness case is where only accuracy is required in both directions.

The numerical values of maximum controller stiffness values (gains) were chosen based on the Eigen values of the passive stiffness matrix of the finger at the center of the 9 points (middle row of middle column) assuming it to be the nominal configuration of the finger.

To further explain the cause of instability we overlaid the passive and controller stiffness ellipses on top of each other. We also performed step response simulations within three of the nine points to validate our analysis. Step response analysis was chosen as it can be considered one representation of environmental interactions and more reliable and repeatable than external impacts.

At different joint configurations, it is noticeable that a constant value of controller stiffness is not stable everywhere in the workspace. The shape of the stable workspace also changes with different values of controller gains (stiffness). This is because the passive stiffness rotates and scales due to the configuration dependency and causes the controller stiffness to go out of passive bounds leading to a poor utilization of the overall workspace. While Fig. 2(c) utilized

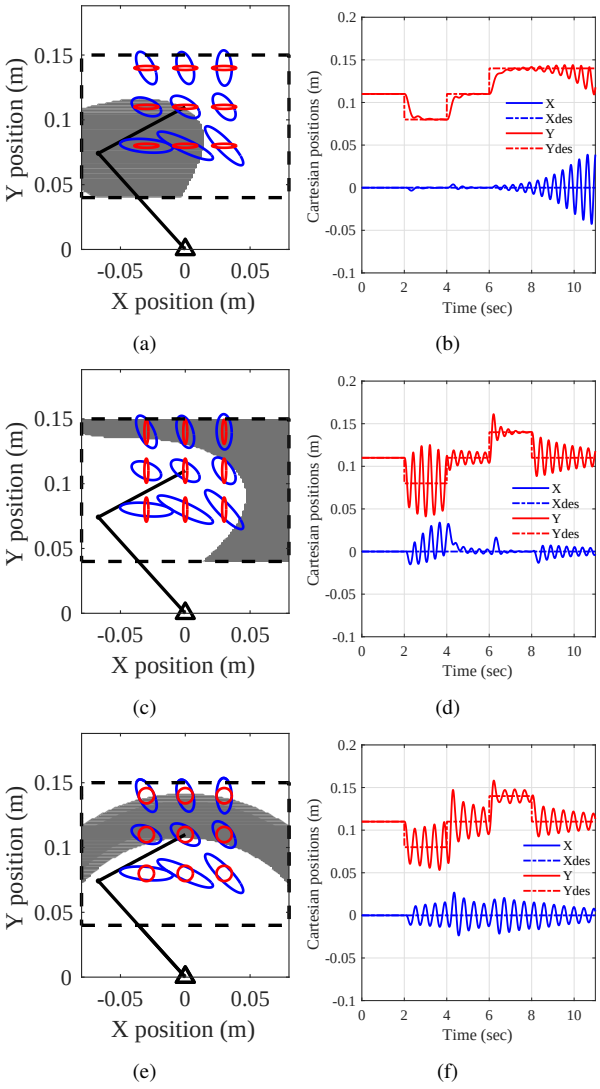

Fig. 2. Stable workspace for fixed Cartesian controller stiffness for a 2DOF planar tendon driven robotic finger. Overall workspace under scrutiny is shown in dotted lines. Shaded regions depict the stable regions while white regions are unstable. Stiffness ellipses for the passive stiffness (blue) and controller stiffness (red) are overlaid. Three cases are shown: (a). High stiffness in x and low stiffness in y, (c). High stiffness in y and low stiffness in x and (e). Equal stiffness in x and y. The ellipses show that instability is caused by controller stiffness crossing the bounds of passive stiffness. A general reduction in overall workspace is observed. Corresponding simulation of steps are shown within the coordinates of the middle column of the ellipses in each plot shown in (b), (d) and (f).

$\sim 40\%$ of the overall workspace, Fig. 2(a) and 2(e) were able to utilize only $\sim 37\%$ and $\sim 34\%$ respectively.

We performed step response analysis of our system with similar masses, inertias and stiffnesses as our experimental platform while keeping the damping low.

While the results apply to step responses in every direction, for the scope of this work, we move in y-direction steps of Cartesian coordinates within the middle column of our selected nine points. The steps start from the nominal position (middle row of middle column), move to an extreme, return back to nominal and move to the other extreme. Fig. 2(b), Fig. 2(d) and Fig. 2(f) clearly exhibit the instability

at different regions in the workspace.

Manipulating objects leads to loading reaction forces as a result of grip forces generated by the fingertips. Such forces lead to the effects of CCT on the stiffness transformations and hence modify the stability boundaries. As the object is moved around and grip forces are changed, the magnitude and angle of such loading forces will change as well leading to further non-linearities.

C. Stable Workspace of Loaded Fingers

We carry out analysis in the presence of external loading forces. From the previous section, we pick the isotropic stiffness case as it is the worst case scenario in terms of workspace utilization and applied a constant force of $1.5N$ at the fingertip at three different angles ($-30°$, $0°$ and $30°$). The angles were chosen based on an estimation of the stable grasp friction cone constraints [10].

We performed similar analysis and simulation as the previous section (Fig. 3). Analysis shows that stability boundaries are indeed modified by loading force magnitudes, directions and finger configurations. While stable workspace area increased for forces at $0°$ ($\sim 48\%$) and $-30°$ ($\sim 63\%$) from the unloaded 34%, there was a decrease in the stable workspace for force acting at $30°$ (26%). For simulations, the controller was modified to include a feed-forward term to compensate for the external forces to maintain the same position in the workspace. The modified controller is expressed as

$$\boldsymbol{\tau_d} = \mathbf{J^T(q)(K}_{x,d}(\mathbf{x_d - x}) - \mathbf{f}_{ext}) \tag{16}$$

Simulations show that the presence of external loading forces play a big role in the performance and stability of Cartesian stiffness control. Certain directions of forces may seem beneficial to the stability due to the forces assisting the controller and thus reducing controller forces. However external loading forces during manipulation are dynamic and change with object states hence making it non-trivial to utilize them for stability.

Our interest lies in the effect of mechanical design elements such as various arrangements of compliance on controller stability. In some of our previous work [8], [9], we identified parallel compliance (PC) as a design element that can be optimized to improve stability while enjoying all the benefits of a compliant transmission.

IV. Optimizing Parallel Compliance for Improving Stability

While increasing series stiffness would increase stability boundaries, it would also lead to a reduction in actuator decoupling and unwanted high passive stiffness in Cartesian directions reducing the overall robustness of the robot. We present a solution to improve stability by adding passive parallel compliance at the joints while maintaining the benefits of a compliant transmission. We optimized the stiffness of a constant diagonal (joint-wise independent) PC term in Eq. (1) to satisfy the stability criteria (Eq. (10)) with the transformations (Eq. (1) and (12)) for all points in our task workspace (nine points).

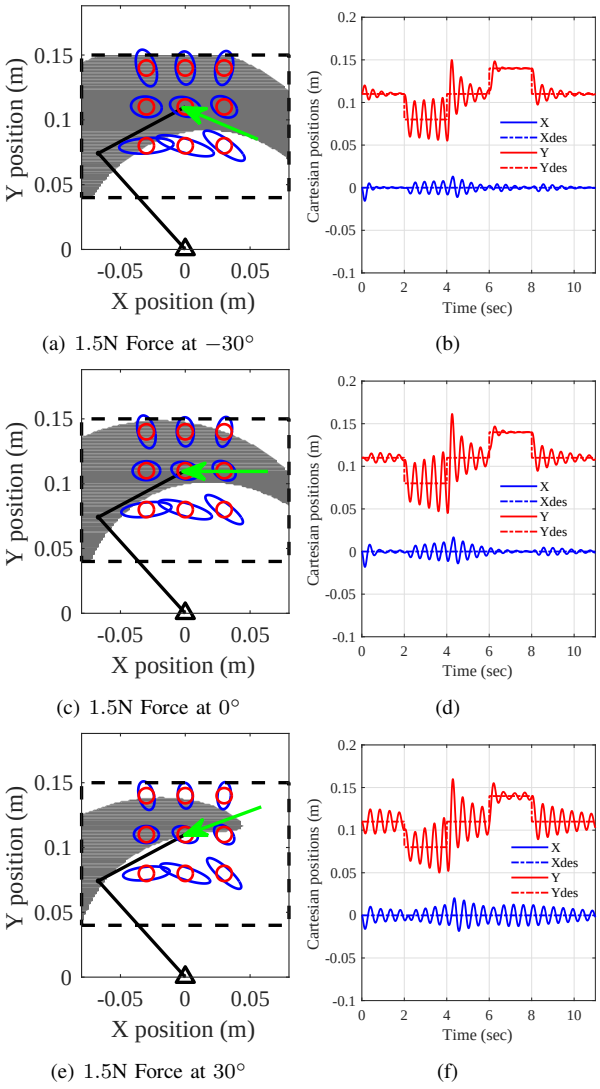

(a) 1.5N Force at $-30°$ (b)

(c) 1.5N Force at $0°$ (d)

(e) 1.5N Force at $30°$ (f)

Fig. 3. Effect of constant load forces on the stable workspace of Cartesian controllers with isometric stiffness. Shaded regions represent the stable workspace for 1.5N loading force acting at the fingertip at three angles:$-30°$ (a) and (b), $0°$ (c) and (d) and $30°$ (e) and (f). Step response was analyzed for three out of the nine points in the middle column. A force at a positive angle decreases stability while a force at a negative angle assists the controller and hence seems more stable.

Our optimization criteria is as follows,

$$\begin{aligned} &\text{minimize} \quad \sum(\text{diag}(\mathbf{K_{pc}}))^2 \\ &\text{subject to} \quad \text{Re}(\boldsymbol{\lambda_i}) > \epsilon, i = 1, \ldots, n. \end{aligned} \tag{17}$$

where λ_i is the vector of Eigenvalues of the stability condition (Eq. 10) and ϵ is a very small positive real number which can be treated as a safety factor. As the inequality is a test of positive definiteness, we want to choose PC stiffness such that the real part of the Eigenvalues of the stability condition are always positive for every point (i) in our desired workspace (n). We minimized the stiffness of the PC element. Note that high values of PC stiffness leads to increased actuator effort and might lead to actuator saturation reducing performance.

For the unloaded finger, we chose the worst case scenario

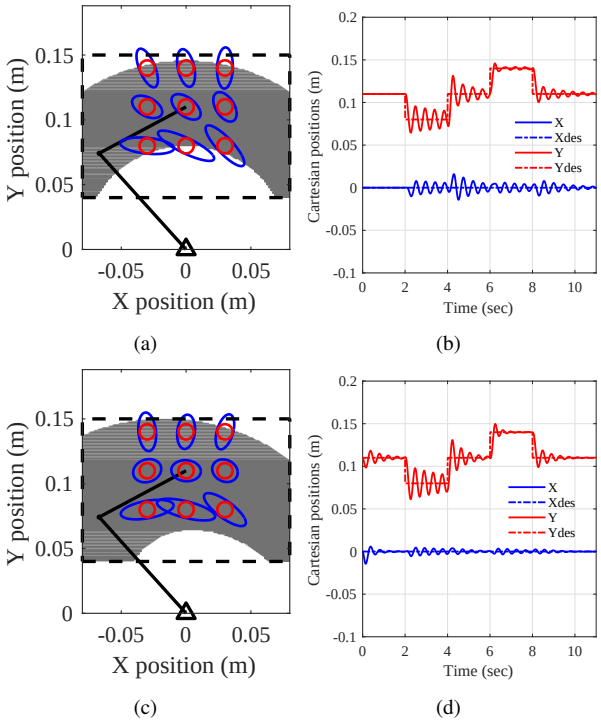

Fig. 4. Effect of addition of optimized parallel compliance for loaded and unloaded fingers with isometric Cartesian stiffness. The unloaded finger (a) and (b) show an increase in stable workspace and comparatively stable step response. The loaded finger (c) and (d) also show improvements in stable workspace and step response.

(isometric stiffness) for optimizing PC stiffness. For simulations, the controller (Eq. (13)) was modified by adding a feedforward term to compensate for the additional joint torque due to the parallel compliance.

$$\boldsymbol{\tau_d} = \mathbf{J^T(q)(K_{x,d}(x_d - x) - f_{ext}) + K_{pc}(q - q_0)} \tag{18}$$

where $\mathbf{q_0}$ is the resting angle of the PC spring.

Analysis and simulations with the optimized PC element added to the system (Fig. 4(a)) showed an increase in stable workspace ($\sim$ 67%) and an overall improvement in step response(Fig. 4(b).

Similarly, we chose the worst case for the loaded finger (1.5N at 30°). Analysis with the optimized PC element (Fig. 4(c)) showed an improvement in stable workspace ($\sim$ 84%) and a highly stable step response(Fig. 4(d)).

Hence, it is clear that parallel compliance can be added to improve the stability of robotic fingers running Cartesian stiffness controllers.

V. Experimental Validation

In order to experimentally validate our analysis and simulations, we designed a planar 2-DOF, 2N tendon driven robotic finger (Fig. 1(b)).

A. Experimental setup

The robotic finger testbed was designed using laser cut acrylic to keep the weights and inertias as low as possible. Bearings were utilized to minimize the effects of damping/friction. High strength fishing line was used for tendons to avoid tendon stretch. Series springs with a stiffness of 718 N/m were attached to each tendon which were then connected to two brushed DC gearmotors (Maxon motors) in a belt drive arrangement. The motors were controlled by Maxon EPOS motor controllers which were setup for closed loop position control tuned to behave like first order systems with a rise time of 0.044 seconds. Two high resolution rotary encoders (US Digital) were used to estimate joint angles. The higher level Cartesian stiffness controller was written in Labview (National Instruments) and was executed on an FPGA controller (NI Compact RIO). Motor pulleys were 57 mm in diameter and joint pulleys were all 34 mm in diameter. The finger was loaded by hanging weights using a pulley attached sufficiently far such that the angle of the load was within $\pm 5°$ of the target of $\pm 30°$.

B. Experimental Results

Step response experiments similar to the simulations used in previous sections were performed with the isometric stiffness equal to that used in the analysis (35 N/m in x and y). The numerical values of controller gains were calculated using the Eigenvalues of the passive stiffness matrix of the finger at the nominal position (middle row of middle column). Experiments were performed for both loaded and unloaded cases with and without PC springs. Torsional PC was achieved by using two linear springs of equal stiffness (k_{pc}) and attaching them to the joint pulley and grounding them on the ground for joint 1 and on joint 1 for joint 2 respectively. The effective stiffness due to such an arrangement ($K_{pc,eff}$) can be calculated as,

$$K_{pc,eff} = 2 * r_j^2 * k_{pc} \tag{19}$$

where r_j is the radius of the joint pulley.

Experimental results (Fig. 5) show that the real system is generally more stable than the simulated system. This is primarily because of unmodeled friction and stiction in the experimental system which dissipates energy and thus makes the system seem more stable.

For the unloaded finger (Fig. 5(a)), results show that the system is less stable when moved to the unstable regions according to the analysis. Optimizing parallel compliance led to us using 40 N/m springs at the first joint and 60 N/m springs at the second. Just as we predicted, the addition of parallel compliance improves the performance of the finger greatly (Fig. 5(b)).

For the loaded finger, we hung a weight of 150 g from a string tied to the finger tip to generate a force of $\sim$ 1.5 N at an angle of 30° and the response was stable but similar to our predictions (Fig. 5(c)). Addition of parallel compliance led to a very stable response without loss in performance (Fig. 5(d)). Optimization gave us springs of stiffness 240 N/m at the first joint and 60 N/m at the second joint.

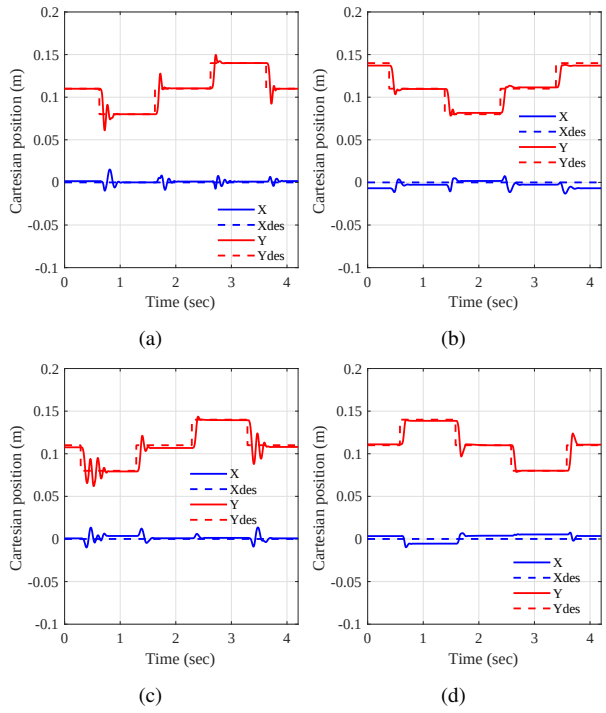

Fig. 5. Experimental step response results. (a) and (c) show response of the unloaded and loaded system respectively without parallel compliance. Addition of parallel compliance leads to improvement in both loaded ((b)) and unloaded ((d)) cases.

VI. Conclusions

In this work, we derived a generalized conservative stability criteria for multi-DOF tendon-driven robotic hands implementing Cartesian stiffness control. A major contribution of this work is that unlike previous research which only considered robots with decoupled passive joint stiffness, our analysis also applies to robots with coupled passive joint stiffness such as tendon-driven robots. These stability bounds apply to robots with any number of DOFs and any type of tendon routing strategies. By workspace analysis we showed that a constant controller stiffness may not be stable everywhere in the workspace due to the dependency of such controllers on robot configuration. This leads to a poor utilization of the available workspace unless very low controller stiffnesses are chosen. Further we showed that loading forces make the stability boundaries highly nonlinear. As object manipulation requires accurate force magnitude and direction control, such nonlinearities are detrimental to dexterity. Using the derived stability bounds, we developed a method to choose an optimal set of constant stiffness parallel compliance to increase the stable workspace and improve performance for both loaded and unloaded fingers. We then experimentally validated our analysis using a robotic testbed. Addition of parallel compliance greatly improved the performance of Cartesian stiffness control with minimum changes to the original controller. Such methods can be used to design robotic hands that are intrinsically stable by virtue of design.

While we chose to optimize parallel compliance, other mechanical design parameters can be optimized such as routing pulley radii and link lengths for intrinsic stability. Also, for existing robots which cannot be physically modified, similar analysis can be used to find the controller stiffness that will lead to stability for a given task workspace essentially making our work applicable to both new and existing robotic hands.

The derived stability boundaries do not consider the effects of dynamic parameters such as mass, inertia and damping which have pronounced effects on stability and thus should be considered as conservative. Designers should consider these stability boundaries as the minimum satisfiable conditions and keep in mind that the real-world systems have unmodeled dynamic features which may lead to modified (usually larger) boundaries compared to theoretical analysis.

Finally, our method focuses on identifying the optimal value of parallel springs with constant stiffness. But this approach may not be optimal in terms of energy consumption as the actuator has to work more to compensate for the torques due to parallel compliance. Future work would include optimizing for non-linear parallel compliance which are a function of joint angles so that we can minimize the overall passive stiffness of the robot at every configuration. Another strategy can be to optimize the resting lengths of the parallel compliance to activate only when required for ensuring stability.

References

[1] A. M. Okamura, N. Smaby, and M. R. Cutkosky, "An overview of dexterous manipulation," in *Proceedings 2000 ICRA. Millennium Conference. IEEE International Conference on Robotics and Automation. Symposia Proceedings (Cat. No.00CH37065)*, vol. 1, 2000, pp. 255–262 vol.1.

[2] R. R. Ma and A. M. Dollar, "On dexterity and dexterous manipulation," in *2011 15th International Conference on Advanced Robotics (ICAR)*, June 2011, pp. 1–7.

[3] A. Albu-Schaffer, M. Fischer, G. Schreiber, F. Schoeppe, and G. Hirzinger, "Soft robotics: what cartesian stiffness can obtain with passively compliant, uncoupled joints?" in *Intelligent Robots and Systems, 2004. (IROS 2004). Proceedings. 2004 IEEE/RSJ International Conference on*, vol. 4, Sept 2004, pp. 3295–3301 vol.4.

[4] A. Albu-Schäffer, C. Ott, and G. Hirzinger, *A Unified Passivity Based Control Framework for Position, Torque and Impedance Control of Flexible Joint Robots*. Berlin, Heidelberg: Springer Berlin Heidelberg, 2007, pp. 5–21.

[5] A. Ajoudani, N. Tsagarakis, and A. Bicchi, "On the role of robot configuration in cartesian stiffness control," in *Robotics and Automation (ICRA), 2015 IEEE International Conference on*, May 2015, pp. 1010–1016.

[6] P. Rao, G. Thomas, L. Sentis, and A. Deshpande, "Analyzing achievable stiffness control bounds of robotic hands with coupled finger joints," in *IEEE Internation Conference on Robotics and Automation (ICRA)*, 2017.

[7] S.-F. Chen and I. Kao, "Conservative congruence transformation for joint and cartesian stiffness matrices of robotic hands and fingers," *The International Journal of Robotics Research*, vol. 19, no. 9, pp. 835–847, 2000.

[8] T. Niehues, P. Rao, and A. Deshpande, "Compliance in parallel to actuators for improving stability of robotic hands during grasping and manipulation," *International Journal of Robotics Research*, 2014.

[9] P. Rao, T. D. Niehues, and A. D. Deshpande, "Effect of parallel compliance on stability of robotic hands with series elastic actuators," in *ASME 2015 Dynamic Systems and Controls Conference, Columbus, Ohio*, Oct 2015.

[10] J. Kerr and B. Roth, "Analysis of multifingered hands," *The International Journal of Robotics Research*, vol. 4, pp. 3–17, 1986.